Electrostatic stiffening and induced persistence length for coassembled molecular bottlebrushes

Storm, I. M., Stuart, M. A. C., de Vries, R., & Leermakers, F. A. M.

Electrostatic stiffening and induced persistence length for co-assembled molecular bottlebrushes

Ingeborg M. Storm, Martien A. Cohen Stuart, Renko de Vries, and Frans A. M. Leermakers*

Physical Chemistry and Soft Matter,

Wageningen University & Research, Stippeneng 4,

6708 WE Wageningen The Netherlands

(Dated: April 9, 2018)

Abstract

A self-consistent field analysis for tunable contributions to the persistence length of isolated semi-flexible polymer chains including electrostatically driven co-assembled DNA-bottlebrushes is presented. When a chain is charged, i.e. for polyelectrolytes, there is, in addition to an intrinsic rigidity, an electrostatic stiffening effect, because the electric double layer resists bending. For molecular bottlebrushes there is an induced contribution due to the grafts. We explore cases beyond the classical phantom main-chain approximation, and elaborate molecularly more realistic models wherefore the backbone has a finite volume, necessary for treating co-assembled bottlebrushes. We find that the way in which the linear charge density or the grafting density is regulated is important. Typically, the stiffening effect is reduced when there is freedom for these quantities to adapt to the curvature stresses. Electrostatically driven co-assembled bottlebrushes, however, are relatively stiff because the chains have a low tendency to escape from the compressed regions because the electrostatic binding force is largest in the convex part. For co-assembled bottlebrushes the induced persistence length is a non-monotonic function of the polymer concentration: for low polymer concentrations the stiffening grows quadratically with coverage; for semi-dilute polymer concentrations the brush chains retract and regain their Gaussian size. When doing so they loose their induced persistence length contribution. Our results correlate well with observed physical characteristics of electrostatically driven co-assembled DNA-bio-engineered protein-polymer bottlebrushes.

---

* frans.leermakers@wur.nl

I. INTRODUCTION

The persistence length l_p of double stranded DNA (dsDNA), that is the length below which DNA can be seen as a rod and above which it is a coil[1], has a value of 50 nm. dsDNA has two charges per base pare, which amounts to a high linear charge density of $v = -6$ charges per nm contour length. Obviously, the double helix gives the DNA its intrinsic stiffness but due to its charge there is an ionic strength dependent contribution as well. The intrinsic rigidity, measured at high ionic strengths, may be as low as 30 nm[2]. The charge on the DNA sets up a diffuse layer of co- and counterions. Such electric double layer resists bending and hence contributes to the bending rigidity by an amount known as electrostatic stiffening. The electrostatic stiffening of semi-flexible polyelectrolytes has been analyzed theoretically by Fixman, Skolnick and Odijk [3, 4] and according to these authors grows quadratically with the linear charge density and decreases linearly with ionic strength φ_s (i.e. growth is quadratic with the Debye length). Hence the apparent persistence length of 50 nm should be understood as being composed of a bare and an electrostatic stiffening effect.

Recently, we have reported on the complexation of a bio-engineered protein polymer C_4K_{12} with DNA.[5] This C_4K_{12} is an extremely well defined protein polymer that consists of 12 positively charged lysines (K_{12}) and a 400 aa, randomly coiled collagen-like block (C_4) which forms a water soluble coil that lacks a clear secondary or tertiary structure (and is basically neutral). Opposite charges attract,[6] and therefore the lysine block binds to the DNA chain by electrostatic interactions.[5, 7] The C_4-block points away from the DNA and builds up an extended corona around the DNA. This kind of a topology is referred to as a bottlebrush. Our case, more precisely, is a co-assembled protein-DNA bottlebrush.

It was found that co-assembled DNA-bottlebrushes can have a sufficiently high aspect ratio l_p/D (D is the cross-sectional dimension of the chain) that allows them to reach an ordered state, i.e. they form liquid crystalline phases at high enough DNA-bottlebrush concentrations.[5] That attaching side chains to a backbone can lead to stiffening and potentially to liquid crystalline behaviour, was first elaborated by Fredrickson [8]. He argued that it should be possible to stiffen the flexible main-chain sufficiently to make lyotropic phases. The backbone of our assembled objects, DNA, is by itself already semi-flexible, and hence able to form liquid crystalline phases.[9] From this perspective it may not be too

2

much of a surprise that we were able to also observe liquid crystallinity for the co-assembled bottlebrushes. However, from the many failed experiments in our laboratory to form co-assembled DNA-bottlebrushes with lyotropic properties we know that our recent result[5] is far from trivial.

Much experimental and theoretical work on bottlebrushes is motivated by the potential lyotropic properties. However there are only few reports in the literature. Wintermantel et al. [10], Tsukahara et al.[11], Nakamura et al.[12] and Li et al.[13] showed that bottlebrushes with relative short polystyrene grafts on a flexible methyl methacrylate main-chain make ordered phases at high concentrations. The lack of comparable examples, brings up many questions about the origin of the lyotropicity in this system. Neurofilaments are a prominent example in nature[14–17] which features liquid crystallinity. In this case there is a rigid core from which a triplet of polyampholytic polypeptide chains emerge. As neurofilaments have a very stiff core, the contributions of the grafted chains are possibly only a perturbation (at least at physiological conditions). In order to know, e.g., how our co-assembled DNA bottle-brush relates to the neurofilament case, it is timely to consider the tunable contributions to the persistence length of (charged) molecular bottlebrushes. Our calculations are targeted to unravel and understand stiffening issues for our co-assembled DNA-bottlebrushes. We haste to mention that our results are applicable and relevant for semi-flexible polyelectrolytes and bottlebrushes in general even though parameters are chosen to mimic our experimental system.

Upon co-assembly of the C_4K_{12} chains and DNA, bottlebrushes are formed and the linear charge density along the DNA backbone is reduced. As the charge density of naked DNA is above the Manning condensation limit[18], the reduction of linear charge density is not very important for low C_4K_{12} coverages (an effect not covered by the Fixman-Odijk law[3, 4]), but near stoichiometric binding the decline of the charge density is significant and the electrostatic stiffening effect is largely suppressed. However, the bottlebrush itself also resists bending, and this contribution is known as the induced persistence length.[19, 20] At low coverages, when the grafts are far apart there is little stiffening effect, however, as soon as the side chains overlap laterally and stretch away from the DNA, the rigidity increases. According to the scaling analysis for brushes, the induced persistence length increases quadratically with the grafting density of the side chains ($1/h$, with h the distance between side chains) and also increases quadratically with the length N of the side chains.[19,

3

21] To quantify the contribution of the induced persistence length to the stiffening, it is necessary to also know the proportionality constant. Numerical self-consistent field (SCF) results of Feuz *et al.* [19] proved that the numerical prefactor is unusually small, i.e. of order 10^{-3}. Recently, it has been suggested that this low prefactor can be attributed to the possibility of side chains to translocate from the compressed convex to the expanded concave side of the curved backbone.[21]

When, for bottlebrushes, translocation effects are important to quantify the chain stiffening, it also becomes relevant to account for the finite volume of the backbone. To see this, we can imagine a short side chain permanently grafted to a point on the curved backbone; let that chain be compressed during the backbone deformation. As the chain is short, it cannot reach the uncompressed regions. Very long chains on the other hand will be able to 'travel around' the backbone and then the excluded volume of the backbone is less important. The effect of the finite size of the backbone is expected to be relevant in our DNA-bottlebrush system because the chains that physisorb onto the DNA-backbone are not extraordinary large: the unperturbed coil size of our C_4K_{12} molecules is only about twice the cross-sectional diameter of the DNA chain.[5] Therefore, we will explicitly introduce a finite volume of the backbone in our SCF model calculations.

Andreev and Victorov have analyzed the electrostatic stiffening in a model that goes beyond the phantom main-chain approximation[22]. They considered the case that the backbone has a finite diameter, e.g. relevant for stiffness of worm-like micelles[23] composed of charged surfactants. They fixed the charge on the wormlike micelle such that half the charge is in the compressed convex side and the other half in the expanded concave side of the curved cylinder. They reported large deviations from the Fixman-Odijk predictions especially when the ionic strength is relatively high. Only in the limit of very low ionic strength they recovered the $1/\varphi_s$ dependence for the chain rigidity.[22]

We expect that models that allow for an annealed charge distribution have a lower persistence length than systems for which the charge is quenched. The same applies to the brush. When, upon bending, the chains can rearrange, we expect a low induced persistence length compared to the quenched situation. Below we will introduce models wherein the grafting or charge distribution is regulated in various ways. For co-assembly there is the equilibration of brush-forming chains with the bulk. In such a case the concentration of freely dispersed polymers becomes another tuning parameter for the apparent bending

rigidity of co-assembled molecular bottlebrushes.

It is largely unknown how the above effects (that contribute to the stiffening of the charge driven co-assembled DNA-bottlebrush) compete with each other. For example, which effect dominates in which regime and how the various contributions relate to one another quantitatively. We do not know of computer simulations that have addressed all these issues in a single model. Such comparison is possible using SCF theory for models which disregard the flexibility of the backbone. It should be noted that our results are therefore relevant for the understanding of large length scale bending. This is more appropriate for semi-flexible backbone systems (i.e. for the DNA case) than for very flexible backbones. The purpose of this paper is to use the SCF theory to elaborate on tunable contributions to the persistence length. We will first present how this follows from the analysis of the free energy of the system. We will then elaborate on the SCF theory,[24] mention the main characteristics and prerequisites, and present the molecular models that are used. The results are split up in three subsections. The first one deals with the electrostatic stiffening and how the classical results are modified when more detailed molecular models are introduced. In the second part we discuss the induced persistence length and focus once again on the influence of the finite size of the backbone on the induced rigidity. In the third part we will discuss the self-assembled bottlebrushes and analyze the difference between two models for adsorption and pay attention to the effects in the plateau of the isotherm, where the polymer concentrations increase to semi-dilute values. In the discussion we will consider the results in the context of our co-assembled DNA-bottlebrush experiments.

II. THE SELF-CONSISTENT FIELD THEORY FOR TUNABLE PARTS OF THE PERSISTENCE LENGTH OF SEMI-FLEXIBLE CHAINS.

Below we will elaborate on the self-consistent field (SCF) theory which is used to evaluate the induced persistence length and the electrostatic stiffening. This can be implemented in a discrete two-gradient cylindrical coordinate system which is illustrated in Figure 1. In this coordinate system the variable $r = 1, 2, \cdots, M_r$ specifies grit points in the radial direction whereas $z = 1, 2, \cdots, M_z$ refer to sites in the longitudinal direction (here M_r and M_z the last coordinates used in radial and longitudinal directions, respectively. At the system boundaries reflecting (mirror-like) boundary conditions are implemented. In Figure 1 the
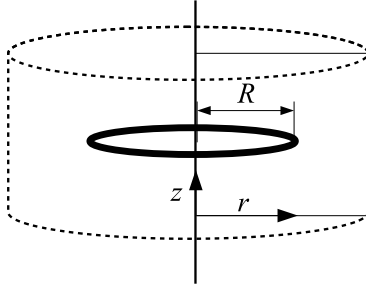
FIG. 1. Illustration of the two-gradient cylindrical coordinate system used in the SCF calculations. The z and r coordinates are indicated as well as the radius of curvature R of the chain which is drawn as a thick black line. Below we will use a lattice model (here not indicated) where the z as well as the r coordinates have discrete values. The mean field averaging is in the radial direction, hence over all sites that have the same (z, r) value (the cross-section grit (z, r) is shown in Figure 2).

black line is the homogeneously curved (main) chain with radius of curvature R. The mean field averaging is performed over sites with the same (z, r) value, that is over $L(r) \propto r$ sites or equivalently the fields are taken to be independent of the angular direction. This approximation is not very good when the side chains are far apart, but it becomes better when the grafted chains are near each other (high grafting density $1/h$, small distance between the side chains, h).

We employ models where excluded-volume effects of the main-chain are introduced in various ways (cf. Figure 2). In particular, our target is to predict the stiffness of co-assembled bottlebrushes that is formed by electrostatic interaction of an ionic copolymer with an oppositely charged backbone, mimicking our experimental DNA-bottlebrush system. Before we focus on the details of the calculations, we need to clearly identify the key characteristics from which these persistence length issues emerge. Therefore we will first briefly visit the thermodynamic background of electrostatic stiffening and induced persistence length calculations.

A. The bending modulus and persistence length of worm-like chains.

One of the key characteristics of a polymer chain is its persistence length.[1, 25] By definition, the persistence length is the length along the backbone below which the direction
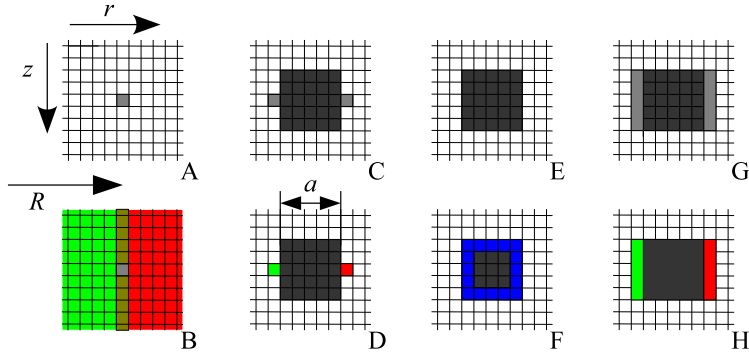
FIG. 2. Illustration of models for the cross-section of the main-chain (backbone) (cf fig. 1). The cylindrical two-gradient coordinate system (z, r) as well as the radius of curvature R of the main-chain are indicated only in panel A (cf Fig. 1) A,B Phantom chains, C-H backbone chain with finite size (here $a = 5$ sites), and segment type S: (A) no constraints; grafts (not shown) emanate from gray site. (B) spatial constraints: half of the chains grafted at gray site have to stay in the red region and other half of the chains are fixed to the green half-space (regions overlap at $r = R$). (C) Chain with fixed size (black): annealed grafting in gray sites. (D) Chain with fixed size: quenched grafting; equal number of chains grafted on green and red site. (E) Chain with fixed size; homogeneous adsorption energy $\chi_S < 0$ for K-stickers. (F) Main chain with fixed size and fixed charge density (blue sites have fixed valency). (G) Chain with fixed size: Annealed charges in gray zones (total charge is fixed). (H) Chain with fixed size: quenched charge distribution. Equal amount of charge in red and green regions. More details are in the text. See also Table I for extra info and how the models are being used.

of the chain is preserved and above which the directions becomes random due to thermal fluctuations. One way to estimate the persistence length in model calculations is to compute the free energy per unit (contour) length that is needed to take a chain and curve it homogeneously with radius of curvature R, and hence impose a curvature $J = 1/R$. When the curvature is a small parameter we can use a Taylor series expansion of the free energy f per unit length, similarly as Helfrich has done for bilayers[26]:

$$f(J) = f(0) + \frac{\partial f}{\partial J} J + \frac{1}{2} \frac{\partial^2 f}{\partial J^2} J^2 + \cdots \tag{1}$$

In this equation the sign of J should not matter and therefore the odd terms must be zero. Therefore we can write

$$f(J) = f(0) + \frac{1}{2} k_c J^2 + \cdots \mathcal{O}(J^4) \tag{2}$$

7

TABLE I. The link between the schematic models given in Figure 2 and the labels used to refer to the models in figs 3, 4 and 6, 7. In this table there is also a brief description of the models used. Volume of the black regions in Figure 2 are inaccessible for the molecules in the solution.

Fig	label	Fig. 2	model description used in SF-SCF calculations
2	Ph	A	"Phantom" chain: The backbone occupies all gray sites of the coordinate at $(z_M/2, R)$. In the refs[3, 4] the main-chain is volume-less.
2	S	F	Even charge distribution around backbone.
2	Q	H	Quenched charge: equal charge density on (green) convex- and (red) concave sides.
2	A	G	Charge on backbone sits on gray sites. The charge is 'Annealed'.)
3	Ph	A	"Phantom" chain: Brush grafted at $(z_M/2, R)$. Backbone is volume-less.
3	Q	D	Quenched grafting. Equal number of chains on (green) convex- and (red) concave sides.
3	A	C	Chains grafted on gray sites: annealed grafting i.e. chains can flip from convex to concave side.
3	H	B	Half the chains are grafted on backbone at the (green) convex- and other half from (red) concave side. Chains can not escape the half-space indicated by the colored regions which overlap by 1 site.
5	solid	F	Even charge distribution around backbone.
5	dashed	E	Homogeneous χ_S around backbone.
6	-	F	Even charge distribution around backbone.

where we introduced the rigidity $k_c \equiv \frac{\partial^2 f}{\partial J^2}$ which has the units $k_B T \times l$ (i.e. energy times length). The rigidity is a direct measure for the persistence length:

$$l_p = \frac{k_c}{k_B T} \qquad (3)$$

because if we curve a piece of the chain with length $2l_p$ with a homogeneous curvature of $J = 1/l_p$ the free energy changes by $(f(1/l_p) - f(0)) \, 2l_p = k_\mathrm{B}T$ which is the thermal energy. After bending such a chain part the tangent of the chain has changed directions by $360/(2\pi) \approx 60°$.

We note that l_p, as introduced above, is relevant for sufficiently stiff semi-flexible main-chains, or in other words, it is the stiffness in the weak curvature limit. We know from multiple computer simulation studies that a flexible main-chain can be rather flexible on the monomer scale and only show its thermodynamic stiffness on larger length scales. In other words, bottlebrushes feature a length scale dependent stiffening.[27–30] Co-assembled DNA-bottlebrushes have an intrinsically semi-flexible backbone and therefore we expect that for this system the large length scale stiffening is the most relevant limit.

In passing we should also mention that the Fixman Odijk predictions[3, 4] and in particular the quadratic scaling of the persistence length with the Debye length has been subject to both experimental, theoretical and simulation studies (see e.g. ref. [31] for an overview). As the early predictions are made in the Debye Hückel limit, it is clear that these do not capture ion condensation effects. Any complication such as the finite thickness of the chain as well as discrete versus smeared charges along the chain introduces a small length scale which must be overcome by the Debye length before the Fixman Odijk predictions are expected to hold. Also intrinsically flexible chains pose a problem. For example, Barrat and Joanny[32] argued that the intrinsic persistence length l_0 of the chain must exceed the value $l_0 > 1/(L_B v^2)$, with L_B the Bjerrum length (approximately 0.7 nm for water) and v the linear charge density, before the Fixman Odijk trend can be expected. It is unknown how charge regulation should enter this picture.

As explained above, our focus here is in the mean field free energy per unit length $f(J)$ which contains the contributions due to the electric double layers (very much in the spirit of Odijk and Fixman) and polymer side chains, the so-called tunable contributions. The intrinsic contribution l_0 is deliberately not accounted for. We will assume that the backbone is sufficiently rigid so that small length scale fluctuations of the backbone are of minor importance. In other words, we focus on the large length scale stiffening only. As the free energy cost of the two backbone bending is relatively independent from the cost of bending double layers or bending the bottle brush, we expect that a superposition rule will apply, that is that the total persistence length is given by the sum of intrinsic one and the tunable

contributions.

B. SCF-machinery and the molecular models

From the above it is clear that we need to evaluate a free energy of the system focusing on electrostatic and polymer brush contributions (the tunable contributions). We will evaluate this free energy using the self-consistent field framework of Scheutjens and Fleer (SF-SCF).[24] These authors suggested to use a lattice to discretize space and use the freely jointed chain model wherein chain molecules are composed of segments that fit the lattice site. Hence such SF-SCF calculations use only one length scale (here and below we will choose a length close to the Bjerrum length,[33] $b = 5 \times 10^{-10}$m) to reduce all linear lengths to dimensionless ones, e.g. the chain length is reduced to the number of segments N (each with size b). We will reduce all energy units by the thermal energy $k_{\mathrm{B}}T = 4 \times 10^{-21}$ J so that the bending modulus k_{c} is directly interpreted as l_{p}.

From the above it is clear that the target of the calculations is a free energy per unit length $f(J)$ as a function of the imposed curvature of a polymer chain $J = 1/R$. Unless specified otherwise the cross-section of the backbone, illustrated in fig 2C-H, is a square of 5×5 lattice sites of segment type S, roughly matching the size of a DNA chain. Segments on the surface of this cross-section may have a fixed charge, quantified by the valency v (fig 2F). In the phantom chain models (fig 2A-B) the volume of the backbone is ignored in the case of the bottlebrush or strongly reduced so that the cross-section is just one segment S with valency v (for models with a line charge).

It will be clear that the exact type of free energy that needs to be used in the Taylor series expansion of Eqn 1 should depend on details of the calculations. When we fix the chemical potential of the molecular species involved, e.g. free polymer or ions, we need to focus on the grand potential $\Omega = F - \sum_i \mu_i n_i$ where F is the Helmholtz energy, μ is the chemical potential and n is the number of molecules and i is an index which runs over all molecular species. For chemically grafted molecular bottlebrushes, however, we need to fix the number of chains per unit length and then the characteristic function is a Helmholtz energy. When we have both permanently grafted chains and freely dispersed ions (for example), it is clear that we have a semi-grand canonical, or partial open canonical ensemble and we will refer to the free energy as free energy partial open.[34] In general the relevant free energy per unit

length f is given by

$$f = \frac{F'}{L} = \frac{1}{L}\left(F - \sum_j{}' \mu_j n_j\right) = \frac{1}{L}\left(\Omega + \sum_k{}'' \mu_k n_k\right) \tag{4}$$

where F' is the characteristic free energy of the system, and L is the length of the backbone. From Eqn 4 it is clear that we can compute the characteristic function in two ways; either starting from the Helmholtz energy and subtracting the chemical contribution terms for all molecules that are mobile and for which the chemical potential is imposed (indicated by the prime on the sum sign), or starting from the grand potential Ω and adding the chemical contribution of all molecular species for which the number of molecules is fixed, e.g. for the grafted chains (indicated by the double prime on the sum sign). It turns out that these thermodynamic quantities are accurately available when the relevant self-consistent field equations have been solved.[24]

Besides thermodynamic information our interest might be on the distribution of molecular species around the backbone chain. In the case of the charged backbone it is the distribution of the ions expressed in dimensionless concentration distributions (also called volume fractions $\varphi_i(\mathbf{r})$, where the value of i may refer to a molecular species). In the field of colloid science the distribution is referred to as the diffuse part of the electric double layer.[35] In the analytical theory the results are obtained in the framework of the Debye-Hückel approximation.[3, 4, 22, 35] We will solve the Poisson Boltzmann equations (on the level of lattice-approximations). Here and below we have a 1:1 electrolyte named Na ($i = 1$, valency $+1$) and Cl ($i = 2$, valency -1) for simplicity reasons. Besides the fact that the ions have a fixed monomer volume b^3, we will assume these ions to be ideal, having athermal interactions with a monomeric solvent W ($i = 0$) and all other molecular components (no specific adsorption energies). In the case of the chemically grafted bottlebrush we consider chains ($i = 4$) with segment ranking numbers $s = 1, 2 \cdots, N$, for which the first segment is constrained to be on a specified coordinate $\mathbf{r} = \mathbf{r}^*$ (phantom model), or a set of coordinates $\mathbf{r}^* \in \{\mathbf{r}_1^*, \mathbf{r}_2^*, \cdots\}$ (cross-section as specified in Figure 2). The distance between the side chains is given by h (in lattice units, a value of $h = 2$ corresponds to 1 nm distance between side chains). We will assume that the solvent quality is good, that is, all Flory-Huggins interaction parameters of the segments with the solvent are set to the athermal value $\chi = 0$.[24, 34, 36] Alternatively, the polymer chains may be freely dispersed in solution and adsorb onto the backbone.

We follow the experimental system closely, which implies that the adsorbing polymers have exactly 12 adsorbing segments (K_{12}) connected to 400 non-adsorbing ones, the so-called C_4 block, specified as C_4K_{12}. Again the solvent quality is strictly kept athermal: $\chi_{WK} = \chi_{WC} = 0$ and also we ignore possible non-zero mixing contributions, i.e. we use $\chi_{KC} = 0$ (and similarly for the interactions with the ions). We consider two models: (i) the fixed adsorption energy case, and (ii) electrostatic binding. Let S denote the unit which specifies the backbone (cf. fig:1). In the context of (i) we realize that adsorption is an exchange process; a solvent molecule is exchanged by a K segment. Hence the effective adsorption energy is given by $\chi_s = \chi_{SK} - \chi_{SW}$. As we set $\chi_{SW} = 0$ the adsorption strength is fully specified by χ_{SK}. Typically, the value of this parameter is negative for adsorption and one needs to divide by 6 to obtain the adsorption energy in units of k_BT (the value of 6 is related to the fact that a cubic lattice is used). In the context of (ii) we consider electrostatic binding energy. Now the backbone surface has a negative charge density, specified by the valency of the S group $v < 0$. This value is fixed, where it is understood that fractional charges are allowed: e.g. a value of $v = -1/2$ means that every other surface group carries a negative charge. The valency of the K segment is $v_K = +1$. We stress that in the case of electrostatically driven adsorption no specific adsorption energy is included. The bulk concentration of polymer is a free (input) parameter.

Summarizing the above, we typically consider segment type X distributions $\varphi_X(\mathbf{r})$ where $X = W$, Na, Cl, C, K, S (only the distribution of S is fixed during the calculations). In the SCF approach we have for each segment type X a conjugate, so-called segment potential $u_X(\mathbf{r})$ distribution. The mean field free energy is a functional of both types of fields $F = F(\varphi, u)$. The electric double layer is typically solved for ions being point charges. In the lattice approach we will go beyond this level of approximation and allow ions also to occupy lattice sites. In such a case the optimisation of the free energy requires a compressibility relation. Typically, we will assume that the system is (even locally) incompressible, that is, for each coordinate $\mathbf{r}$ we require that the sum of the volume fractions equals unity, i.e.,

$$\sum_X \varphi_X(\mathbf{r}) = 1 \tag{5}$$

and the free energy functional as used in the SF-SCF approach read

$$F = -\ln Q(\{u\}) - u \cdot \varphi + F^{\text{int}}(\{\varphi\}) + \alpha \left(\sum_X \varphi_X - 1 \right) \tag{6}$$

12

where we omitted spatial coordinates for simplicity, and employ the notation $u \cdot \varphi = \sum_{\mathbf{r}} \sum_X u_X(\mathbf{r}) \varphi_X(\mathbf{r})$. Q is the partition function of the system which in the mean-field approximation[34] can be decomposed as $Q = \Pi_i q_i^{n_i}/n!$ with single chain (molecular) mean-field partition functions $q = q(\{u\})$, which can be computed when all segment potentials $u_X(\mathbf{r})$ are known. The free energy of interaction F^{int} should contain all interactions that are experienced by the molecules. In the current calculations just two contributions are accounted for: the first is (i) the adsorption energy for the segments of type K for the surface (in the case of the adsorption of C_4K_{12}). Only when the distance between a segment K and a surface site S (from the backbone) is exactly unity (lattice unit b) the adsorption energy is active and the energy of the system changes proportional to the Flory-Huggins parameter χ_{SK}. In fact, as we take the reference for adsorption $\chi_{SW} = 0$, we can interpret $\chi_{SK}/6$ as the adsorption energy in units k_BT when a segment K sits next to the surface S and by doing so displaced a solvent W. The factor $1/6$ comes from using a cubic lattice. (ii) When there are charges in the system we have the usual electrostatic contribution $\frac{1}{2}\epsilon \sum_{\mathbf{r}} E^2(\mathbf{r})$, with $E = -\nabla\psi$ the electric field strength for which it is necessary to evaluate the electrostatic potential ψ. Probably the best electrostatic potentials for the system are found when these are computed using the Poisson equation [37]:

$$\nabla^2 \psi = -\frac{\sigma}{\epsilon} \tag{7}$$

the exact form depends on the geometry (specified below). This form of the Poisson equation is appropriate because we will not allow for gradients in dielectric permittivity ϵ. The charge density distribution is easily obtained from the distribution of the ionic species in the system:

$$\sigma(\mathbf{r}) = e \sum_X \varphi_X(\mathbf{r}) v_X \tag{8}$$

with e the elementary charge. The final term in the mean field free energy functional, Eqn 6, is a Lagrange multiplier for each coordinate $\alpha(\mathbf{r})$ which is coupled to the incompressibility relation.

The first goal is to find the optimal segment potential and segment density distributions so that the mean-field free energy is at an extremum. It turns out that the free energy must be maximized with respect to the segment potentials and the Lagrange field and minimized with respect to the volume fractions. Hence a saddle point is needed. This optimization must be done numerically.[38] In practice we search iteratively to find a situation for which

13

the first derivatives of the free energy are zero:

$$\frac{\partial F}{\partial \varphi_X(\mathbf{r})} = -u_X(\mathbf{r}) + \frac{\partial F^{\text{int}}}{\partial \varphi_X(\mathbf{r})} + \alpha(\mathbf{r}) = 0 \tag{9}$$

$$\frac{\partial F}{\partial u_X(\mathbf{r})} = -\frac{\partial \ln Q}{\partial u_X(\mathbf{r})} - \varphi_X(\mathbf{r}) = 0 \tag{10}$$

$$\frac{\partial F}{\partial \alpha(\mathbf{r})} = \sum_X \varphi_X - 1 = 0 \tag{11}$$

From Eqn 10 we obtain the rule how to compute the best volume fractions φ_X. From Eqn 9 we obtain how to compute the best potentials u_X and when we obey to Eqn 11 we know that the Lagrange field is optimal. We can easily rewrite Eqn 9 and arrive at an expression for the segment potential. Physically $u_X(\mathbf{r})$ is the work needed to bring a segment X from the bulk to the position $\mathbf{r}$. This quantity is normalized by the thermal energy so that the segment potential is dimensionless. The result is a lattice variant of the Boltzmann weight as used in the Poisson Boltzmann theory, augmented with a specific adsorption energy contribution and a term which accounts for the finite size of the segments:

$$u_X(\mathbf{r}) = \alpha(\mathbf{r}) + \frac{v_X e \psi(\mathbf{r})}{k_{\text{B}} T} + \chi_{SX} \langle \varphi_S(\mathbf{r}) \rangle \tag{12}$$

The angular brackets in this equation will be discussed below in more detail. Here it suffices to mention that the last term of Eqn 12 is only non-zero when the coordinate $\mathbf{r}$ neighbors a surface site S (for which all positions are specified) and then has the value $\lambda_1 \chi_{SX} = \chi_{SX}/6$. Again, the third term only is present when we consider the physisorption of $C_4 K_{12}$ chains with a fixed adsorption energy. The second term only exist when there are charges in the system. The first term in the segment potential is there in all cases and is the only term when a brush on uncharged segments is considered. Both the electrostatic potential ψ as well as α approach zero in the bulk. The classical Poisson-Boltzmann approach follows from Eqn 12 by ignoring the volume of the ions: only the second term survives in this case.

The evaluation of the volume fraction distribution, which obeys the rule Eqn 10, depends on the chain model that is used. Ideally one would like to use a self-avoiding chain as this model is most accurate with respect to the excluded-volume interactions. Such a model can only be implemented for very short chains. Here we have used the freely jointed chain (FJC) model[25] for which there exists an efficient propagator formalism to evaluate the single-chain partition function and corresponding volume fraction distributions (see below). In the FJC model we ignore bond orientation correlations even between two neighboring

bonds. The only requirement that is implemented is that two neighboring segments along the chain occupy neighboring lattice sites. Such FJC model thus allows for chain backfolding events. We recall that this is fully in the spirit of the mean-field approximation as exemplified by the focus on the evaluation of single-chain partition functions, which (obviously) ignores inter-chain crossings. The incompressibility relation of Eqn 5 is there to correct for these unrealistic situations. Indeed this constraint makes sure that each lattice site, on average, is occupied only once by a segment of a polymer, a solvent or ion molecule and that at the position occupied by the backbone no other segments can be placed. Hence, inter- as well as intra-molecular excluded-volume effects are handled on the same (approximate) footing.

We now briefly outline how to find, starting from the segment potentials the distribution of the molecules. For obvious reasons we need a notation to specify which segment of the chain is of which type. For this we introduce $\delta_{i,s}^A$, which takes the value unity when segment s of molecule i is of type A and is zero otherwise. All δ values are known from the input. First, we generalize the segment potential to be dependent on the segment ranking number by

$$u_i(\mathrm{r}, s) = \sum_A \delta_{i,s}^A u_A(\mathrm{r}) \tag{13}$$

Next, we compute the segment Boltzmann weight $G_i(\mathrm{r}, s) = \exp -u_i(\mathrm{r}, s)$ and refer to it as the free segment distribution function. As the potentials are zero in the bulk reference phase, the Boltzmann weights are unity in the bulk. We note that the distributions of the monomeric species $m \in \{Na, Cl, W\}$ already follow from such free segment distribution functions:

$$\varphi_m(\mathrm{r}) = C_m G_m(\mathrm{r}, 1) \tag{14}$$

because these molecules are just one segment long. In grand canonical calculations the value of the bulk volume fraction φ_m^b is known and then $C_m = \varphi_m^b$. Note that in the classical Poisson-Boltzmann theory the very same Boltzmann equation is used to find the distribution of the ions.[35] We note that also in the bulk the system has to obey to the compressibility relation as well and we have

$$\sum_X \varphi_X^b = 1 \tag{15}$$

and typically the volume fraction of the solvent in the bulk is computed from $\varphi_W^b = 1 - \sum_{j \neq W} \varphi_j^b$. When there are charged segments or ions in the system, it must be true that the

bulk is electroneutral:

$$\sum_X \varphi_X^b v_X = 0 \tag{16}$$

This means that the volume fraction in the bulk of one of the ion species can not be given by the input, but is computed from the electroneutrality constraint (Eqn 16). Typically the bulk concentration of the other ion is used to set the ionic strength.

The next step is to consider so-called end-point distribution functions of the type $G_i(\mathbf{r}'', s''|\mathbf{r}', s')$,[39] which specify the combined statistical weight of all possible conformations of chain fragments that start with segment s' at coordinate $\mathbf{r}'$ and finish at segment s'' at coordinate $\mathbf{r}''$. Clearly, when $s' = s''$, it is necessary that $\mathbf{r}' = \mathbf{r}''$ and the end-point distribution function is given by the free segment distribution function, i.e., $G_i(\mathbf{r}'', s'|\mathbf{r}', s') = G_i(\mathbf{r}', s') = G_i(\mathbf{r}'', s'')$. We can integrate over 'starting' positions: $G_i(\mathbf{r}'', s''|s') = \sum_{\mathbf{r}'} G_i(\mathbf{r}'', s''|\mathbf{r}', s')$. In the propagators two of such (integrated) end-point distribution functions are used, namely one for which the starting segment is $s' = 1$, $G_i(\mathbf{r}'', s''|1)$ and the other one for which the starting segment is $s' = N$, $G_i(\mathbf{r}'', s''|N)$. At this point we realize that the double primes are no longer necessary and we drop these from our notation. The end-point distributions are generated by the propagators, which are discrete implementations of the Edwards diffusion equation,[40] by extending the chain fragment with one segment.

$$G_i(\mathbf{r}, s|1) = G_i(\mathbf{r}, s) \sum_{\mathbf{r}'}^{*} \lambda_{\mathbf{r},\mathbf{r}'} G_i(\mathbf{r}', s-1|1) = G_i(\mathbf{r}, s)\langle G_i(\mathbf{r}', s-1|1)\rangle \tag{17}$$

$$G_i(\mathbf{r}, s|N) = G_i(\mathbf{r}, s) \sum_{\mathbf{r}'}^{*} \lambda_{\mathbf{r},\mathbf{r}'} G_i(\mathbf{r}', s+1|N) = G_i(\mathbf{r}, s)\langle G_i(\mathbf{r}', s+1|1)\rangle \tag{18}$$

which defines the angular brackets. Here $\lambda_{\mathbf{r},\mathbf{r}'}$ are *a priori* step probabilities which are taken according to the geometry of the system and are consistent with the FJC model. As in the FJC the two neighboring segments must be on neighboring lattice sites, we realize that the sum is only necessary over coordinates $\mathbf{r}'$ that neighbor coordinate $\mathbf{r}$. This is indicated by the asterisk above the sum sign. The transition probabilities add up to unity as $\sum_{\mathbf{r}'}^{*} \lambda_{\mathbf{r},\mathbf{r}'} = 1$. When a three-gradient Cartesian coordinate system is used, i.e. $\mathbf{r} = (x, y, z)$, we can use a cubic lattice and then set all λ-values to $1/6$. By readjusting the initialization of the propagators, we can implement the grafting condition for the polymers. Below we will, for such case, focus on the situation that the first segment is not free to go to all possible positions. Typically the first segment is placed only on a subset of coordinates. Let these

pinning coordinates given by the set $\{\mathbf{r}_\mathrm{p}\}$ (again specified by the input). Then the starting of the forward propagator reads

$$G_i(\mathbf{r}, s|1) = G_i(\mathbf{r}, 1)\delta_{\mathbf{r},\mathbf{r}_\mathrm{p}} \tag{19}$$

wherein $\delta_{\mathbf{r},\mathbf{r}_\mathrm{p}} = 1$ when $\mathbf{r} \in \{\mathbf{r}_\mathrm{p}\}$ and zero otherwise.

We can now evaluate all distributions and thermodynamic quantities, because from the above it will be clear that we can start the propagators by setting $G_i(\mathbf{r}, 1|1) = G_i(\mathbf{r}, 1)$ and $G_i(\mathbf{r}, N|N) = G_i(\mathbf{r}, N)$. After $N-1$ steps we arrive at the other end of the chain and from these end-point distributions we compute the chain partition function. Both for freely floating chains as well as for pinned (grafted) chains we can use

$$q_i = \sum_{\mathbf{r}} G_i(\mathbf{r}, N|1) \tag{20}$$

Very efficiently, the volume fraction distributions of the chain segment are found by combining Eqns 17 and 18 using the so-called composition law:

$$\varphi_i(\mathrm{r}, s) = C_i \frac{G_i(\mathbf{r}, s|1)G_i(\mathbf{r}, s|N)}{G_i(\mathrm{r}, s)} \tag{21}$$

In this equation the division by $G_i(\mathrm{r}, s)$ is necessary to correct for the double counting of the segment weight. The normalization constant C_i can be expressed in terms of the number of molecules in the system n_i in the case of canonical calculations or in terms of the bulk volume fraction in grand canonical calculations:

$$C_i = \frac{n_i}{q_i} = \frac{\varphi_i^b}{N_i} \tag{22}$$

Summarizing, from the above it follows that it is possible to compute the volume fractions as soon as the segment potentials are available (Eqns 14 and 21) and when the segment volume fractions are available we can compute the segment potentials (cf. Eqn 12). As already mentioned, a fixed point of these equations is found routinely in an iterative manner, wherein the potentials are systematically tuned until the volume fractions are found which both follow from the potentials and determine the same potentials, while they obey to the incompressibility relations (Eqns 5 and 15). Routinely we obtain 7 significant digits in order 100 iteration steps.[38] This fixed point is referred to as the self-consistent field solution. For such SCF solution we can compute the free energy using Eqn 6. Other relevant

17

thermodynamic quantities can be computed straightforwardly as the chemical potentials of the mobile components follow from the Flory-Huggins theory [36]

$$\mu_i \equiv \frac{\mu_i}{k_B T} = \ln \varphi_i^b + \ln N_j + 1 - N_i \sum_j \frac{\varphi_j^b}{N_j} \qquad (23)$$

wherein the interaction terms were omitted because in all calculations discussed below the FH χ-parameters were taken to have the athermal value. When, in the bulk, there are only monomeric species the dimensionless FH chemical potential reduces to $\mu_i = \ln \varphi_i^b$.

III.   THE GEOMETRY

The spatial coordinates $\mathbf{r}$ have not yet been specified. The above notation suggests a Cartesian coordinate system $\mathbf{r} = (x, y, z)$, but calculations for such a system are CPU intensive and very time consuming. Making use of symmetry allows us to reduce the number of gradient directions and to implement a mean-field approximation in the other direction(s).[24] The focus here is on a main-chain which is homogeneously curved in one direction. This can be captured in a cylindrical coordinate system with gradients in a radial direction (indicated by the radial layer number r) and a direction along the axis of the cylinder (indicated by a z-coordinate).[19] More specifically (cf. Figure 2 where a small part of the coordinate system is presented) we implement $\mathbf{r} = (z, r)$, wherein r is a radial coordinate $r = 1, 2, \cdots, r_M$, and z is a direction along the long axis of the cylinder $z = 1, 2, \cdots, z_M$. At all system boundaries we have implemented reflecting (mirror-like) boundary conditions, which means that for all end-point distributions and also for the volume fractions and electrostatic potential profiles it is implemented that the gradients at the system boundaries are zero. For example, for the electrostatic potential $\psi(z_M + 1, r) = \psi(z_M, r)$ for all r values and $\psi(z, r_M + 1) = \psi(z, r_M)$ for all z values. Typical values for r_M and z_M is 400.

Such a two-gradient cylindrical coordinate system requires a few modifications of the above equations. The important point is that the number of lattice sites at position $\mathbf{r} = (z, r)$ grows as $L(r) = A(r) - A(r-1) = \pi(2r - 1)$, as we use for $A(r) = \pi r^2$. The angular brackets defined in Eqns 17 and 18, will be modified to account for this geometry. Introducing step probabilities $\lambda_{z,r;z,r-1} = \frac{1}{6} S(r-1)/L(r)$, $\lambda_{z,r;z,r+1} = \frac{1}{6} S(r)/L(r)$ and $\lambda_{z,r;z-1,r} = \lambda_{z,z+1} = 1/6$, so that the step probability which does not change coordinates will have the value $\lambda_{z,r;z,r} = 2/6$ as the circumference $S(r) = 2\pi r$ we can implement the site average of a quantity X at

18

(z, r) by

$$\langle X(z,r) \rangle = \frac{2}{6} X(z,r)$$

$$+ \sum_{i=-1,1} (\lambda(z,r;z+i,r)X(z+i,r) + \lambda(z,r;z,r+i)X(z,r+i)) \tag{24}$$

The partition function is now computed by $q_i = \sum_z \sum_r L(r) G_i(z,r,N|1)$ and the number of grafted chains per unit length along the backbone can be computed from the radial volume fraction profile of the polymer (recall that the polymer has the index $i = 4$):

$$n_4 = \frac{1}{N_4} \sum_z \sum_r L(r) \varphi_4(z,r) \tag{25}$$

This number of chains is straightforwardly converted to the distance h between the grafts, $h = 2\pi R/n_4$.

The length of the torus is found from the central position of the DNA chain in this cylindrical coordinate system. As indicated in Figure 2, the center is at (z', R) and then the length of the backbone chain (curved in a ring or torus) is given by $L = \pi(2R - 1)$ and the curvature is given by $J = 1/R$.

1. Lattice-Noise

We have used Eqn 2 to evaluate k_c and thus l_p. We note that

$$l_p = \frac{k_c}{k_B T} = (f(J) - f(0)) \frac{2}{J^2} \tag{26}$$

So when the reference value for the appropriate free energy per unit length of the chain in the straight configuration $f(0)$ is available, we can evaluate $l_p = 2(f(J) - f(0))R^2$. It must be understood that the use of a lattice is not completely without consequences. It turns out that the evaluation of $f(J)$ as well as $f(0)$ typically include (very small) erroneous contributions due to the lattice (so-called lattice artifacts), implying that any l_p value (as used by Eqn 26) depends slightly on the radius R used in the calculations.[41] That is why the radius of the torus is varied over a significant range and l_p is computed by averaging over these results. In this procedure we found that it is not necessary to compute $f(0)$ explicitly, but we keep $f(0)$ as a 'fitting' parameter: the best $f(0)$ is taken so that l_p estimates are not a function of the explicit range of torus radii used. It was checked that the fitted value of $f(0)$ is indeed consistent with the free energy per unit length of the chain in the straight configuration.
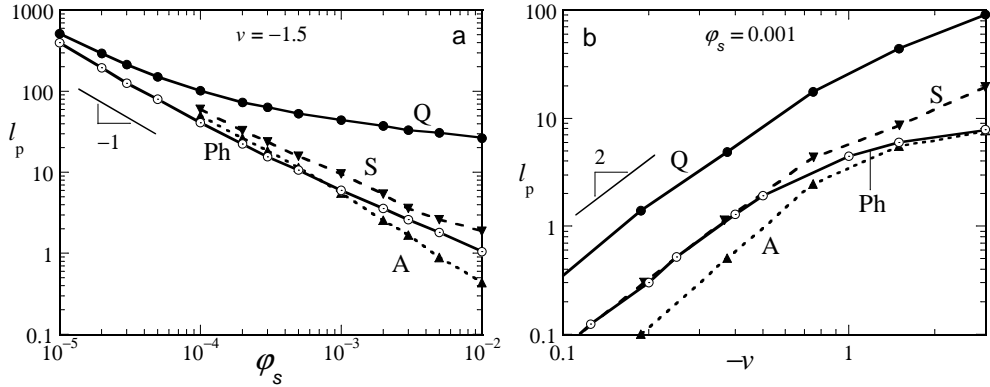
FIG. 3. a) The electrostatic stiffening, l_p in units of lattice sites, as a function of the salt concentration φ_s, for a polymer chain with linear charge density $v = -1.5$ charges per lattice site in log-log coordinates. b) The electrostatic stiffening l_p in units of lattice sites as a function of the linear charge density for a given volume fraction of salt $\varphi_s = 0.001$ in log-log coordinates. Q) is quenched charge density, A) annealed charge density. Ph) the main-chain has minimum volume of one lattice site (phantom main-chain). S) is the fixed surface charge density around the DNA chain. 1:1 electrolyte. All interaction parameters are taken athermal. The indicated slopes give the prediction of Fixman and Odijk.[3, 4] See Figure 2 and Table I for details of the models used.

IV.   RESULTS AND DISCUSSION

Our results will be presented in the following order: (i) electrostatic stiffening of negatively charged backbone chains, which will be compared to the phantom chain predictions of Fixman and Odijk [3, 4] and for backbone chains with volume to Andreev [22]; (ii) the induced persistence length of chemically fixed bottlebrushes and these results will be compared to results of Feuz [19]; (iii) co-assembled bottlebrushes for which the predictions are relevant for our co-assembled DNA-bottlebrushes.

A.   Electrostatic stiffening

In Figure 3 we present our numerical SCF results for electrostatic stiffening. In Figure 3a the electrostatic persistence length is given as a function of the ionic strength in double logarithmic coordinates for a linear charge density of $v = -1.5$ charges per lattice site (which amount to 3 charges per nm, e.g., relevant for ssDNA). In Figure 3b the electrostatic

20

persistence length is given as a function of the charge density v along the chain for a salt volume fraction of $\varphi_s = 10^{-3}$ which is close to the experimentally relevant concentration of 10 mM salt,[5] again in double logarithmic coordinates. The labels on these figures refer to the different models that are used which are pictorially illustrated in Figure 2 and more specifically addressed in Table I. The lines with slope -1 and 2 for the figs 3a and 3b, respectively, are the theoretical Fixman-Odijk predictions.

Our SF-SCF attempt to mimic the Fixman-Odijk predictions is labeled by Ph. As mentioned in Table I this case comes closest to the phantom chain: in SF-SCF the backbone occupies just one ring of lattice sites. Concerning the ionic strength dependence, for low salt concentrations our phantom (Ph) chain is exactly behaving according to the Odijk and Fixman predictions. For high salt we see that our phantom chain is slightly deviating from the -1 slope in Figure 3a. We attribute this deviation to the fact that in SF-SCF there is a finite size of the backbone which brings in a small length scale that is seen as soon as the Debye length becomes sufficiently small (that is at high salt concentrations). With respect to the dependence on the charge density (Figure 3b) we observe the expected scaling value of 2 at low charge density. The leveling off at high charge density is due to the onset of ion condensation. This is to be expected since we solve the full Poisson-Boltzmann equation which correctly accounts for ion condensation while this effect is ignored when the Debye Hückel approximation is used.

The other two models, labelled A and S implement different ways to regulate the charge upon bending. In the annealed (A) case we fix the overall charge per unit length of the chain and allow the charge to be on the inner and outer faces of the backbone core (gray regions in Figure 2G), but upon bending the charge can locally adjust. In the fixed surface charge density (S), there is a 'hidden' regulation, as a curved backbone has more 'surface area' in the concave part than in the convex parts, hence the charge is distributed accordingly. In both cases there is a finite size backbone, but little of that is found back in the ionic strength dependencies. The annealed case follows the Fixman-Odijk prediction in the full range of ionic strengths used. The fixed surface charge (S) case gives a result which is only marginally larger than for the phantom chain (Ph). With respect to the dependence on the linear charge density (Figure 3b), the annealed predictions tend to be a bit lower than the phantom chain results, especially at low charge densities, whereas the fixed surface charge results are a bit higher than the phantom chain results, especially at high charge densities.

We can rationalize these results by realizing that a low charge density benefits more from charge regulation than a high charge density (for curve A), while the case with fixed surface charge density can possibly postpone the ion condensation effect by distributing the charge over a larger surface area.

The main message coming from Figure 3(a) is that assigning a finite volume to the backbone chain does not necessarily affect the electrostatic stiffening behavior of the polymer. The Fixman-Odijk prediction is remarkably robust with respect to the volume of the backbone as soon as some charge regulation is possible. The quenched case is somewhat artificial and the strong deviations are therefore not that important. When we consider the model of DNA (S), we see that the finite size of the double helix with a fixed charge density behaves close to the Fixman Odijk predictions, even though the linear charge density along the chain is slightly beyond the Manning condensation limit. The deviations due to this are hardly noticed from the ionic strength dependence, and make only a marginal correction to the charge density dependence. When we study the co-assembly mechanism, below, we will implement the homogeneous charge density (S) model.

A numerical estimate for the electrostatic stiffening of DNA at approximately 10 mM salt is only about 10 (lattice units), which translates to 5 nm. This value is small compared to an estimate of the intrinsic persistence length of 30 nm. At 1 mM salt, however, the electrostatic contribution has increased to approximately 40 lattice units, or equivalently to 20 nm, and the overall persistence length is then predicted to be 50 nm, rather close to the value often cited in the literature. Experiments below 1mM salt might produce an effective persistence length for DNA which is even larger (e.g. 80 - 100 nm), provided that the double stranded nature is conserved at such low ionic strengths.

B. Induced persistence length

Numerical SCF results for the induced persistence length of chemically grafted bottle-brushes are collected in Figure 4. Here the induced persistence length is given as a function of the chain length of the grafts in double logarithmic coordinates for a distance between grafts of 1 nm, that is for $h = 2$. In the corresponding Figure 4b the induced persistence length as a function of the grafting distance h (in lattice units) in double logarithmic coordinates is given for $N = 400$. The different models are illustrated in Figure 2 and elaborated
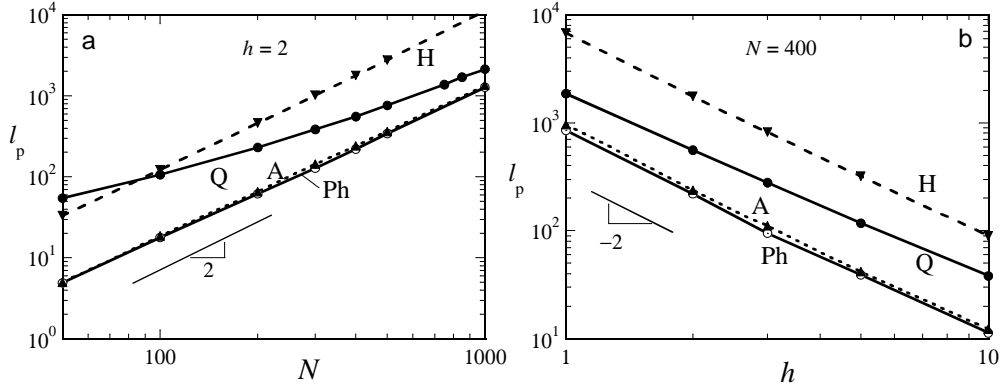
FIG. 4. a) The induced persistence length, l_p in units of lattice sites, as a function of the degree of polymerization of the side chains for a given distance between the grafts $h = 2$ lattice sites in log-log coordinates. b) The induced persistence length l_p in units of lattice sites as a function of the distance between the side chains for a given length of the side chains $N = 400$ in double logarithmic coordinates. Q) is quenched mobility of side chains, A) annealed mobility. Ph) volume of the main-chain is ignored: first segment of the side chains is fixed to $(M_z/2, R)$ (phantom chain). H) is the model in which chains can not translocate with any of the segments from the convex to the concave side. See Figure 2 and Table I for details of the models used. The theoretically expected slopes 2 in panel a and -2 in panel b, are indicated.

on in Table I. Both the phantom chain model Ph and the H model ignore the backbone volume: the first segment of the grafted chains is put at $(z_M/2, R)$. The other models take a finite volume of the backbone into account. To our knowledge such models have not been used in the literature yet.

The numerical result for the phantom chain approximation, that is a bottlebrush for which the backbone volume is completely ignored, labeled by Ph, is very well known and documented.[19] The fitting at sufficiently large N and small h reveals an approximate scaling of $l_p = 0.002(N/h)^{1.9}$. The deviation from the power-law coefficient of 2 is larger when the short chain data are included and less when only the longer chain lengths are used in the fitting. It is remarkable that the numerical coefficient deviates strongly from the expected value of unity. It must be noted that the scaling relations do not account for the translocation of segments, whereas in the numerical SCF results these translocations are allowed and accounted for.

The results labeled by H are computed using a model introduced by Mikhailov et al.

23

[21] to explain why the numerical coefficient for the phantom chain model is dramatically low. In this model half the chains exit from the phantom backbone on the convex and the other half on the concave side of the backbone. In addition, the remainder of the chain segments have to stay at the respective half space, that is, the convex chains must have all their segments in the space with radial coordinates $r \leq R$, whereas the other chains must remain in the region $r \geq R$. This rather artificial model does not destroy the scaling. In fact, it gives results much closer to the analytical scaling predictions. Fitting of the H-curve of these results give $l_{\mathrm{p}} = 0.012(N/h)^{1.99}$. Still, the coefficient is much less than unity, but already 6 times higher than for the phantom chain case. Moreover, the power law coefficient is closer to the expected value of 2. In effect, the difference between persistence lengths of the predictions Ph and H is a factor of 10 over the whole range of N and h values used.

The H model is a rather artificial one. Introducing a finite size of the backbone is a more realistic alternative to put constraints on the ability to translocate segments upon bending from convex to concave parts. In the model Q we present a backbone with fixed volume, and now half the chains are grafted on the convex part and the other half are grafted on the concave side of the backbone. The grafting is quenched, which means that the chains can not move their grafting coordinate from the convex to the concave sides, but unlike in the H model, chain conformations are allowed to cross the $r = R$ coordinate. From Figure 4a we see that $l_{\mathrm{p}}(N)$ deviates strongly from the power law dependence. The reason for this is clear. The finite size of the backbone introduces a new length scale and as long as the thickness of the corona is not large compared to this size we effectively have eliminated the possibility to cross the $r = R$ coordinate. For very short chains the l_{p} approaches the results of H. Indeed the stiffness can even exceed the H-value for very short chains. This effect must be attributed to the volume of the backbone which is excluded for the Q case and not present in the H-model. The longer the chains, the less they notice the backbone and therefore the induced persistence length l_{p} goes to the phantom chain value for large values of N. In Figure 4b results for $N = 400$ are given for which the importance of the backbone is still reasonably large. Also the scaling with respect to h is destroyed by the volume of the backbone. The larger the size of the corona is, the less important is the volume of the backbone and therefore we see that the $l_{\mathrm{p}}(h)$ approaches the phantom chain limit when h is small, and the deviations are largest for large values of h.

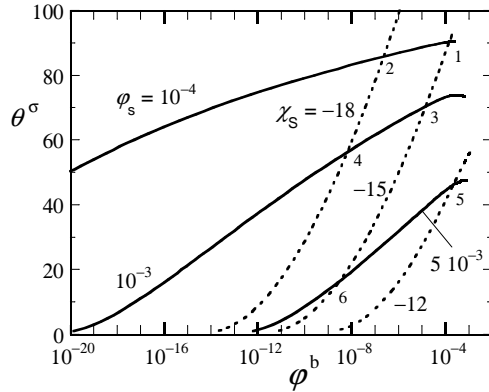The model A where the grafting is annealed is the last one to be discussed. This model

FIG. 5. The adsorbed amount of C_4K_{12} copolymers in number of segments per unit length of the DNA chain as a function of the volume fraction of copolymer in solution in lin-log coordinates. The solid lines are for the electrostatically driven adsorption (Figure 2F, $v = -3$). The ionic strengths $\varphi_s = 1 \times 10^{-4}$; 1×10^{-3}; 5×10^{-3} are indicated. The dashed lines are for the classical case with fixed adsorption energy (Figure 2E)). The adsorption energy $\chi_S = -18$, -15, -12 are indicated. Crossing point of the isotherms are numbered 1-6 and these point represent conditions for which the bending rigidity of the self-assembled bottlebrush are computed which are presented in Figure 6.

has features similar to the quenched case. However, upon bending, the chains can choose to appear on the concave or convex side of the backbone with fixed volume. As can be seen from the results presented in Figure 4, the persistence length is extremely close to the phantom chain values. This is not too surprising because the finite volume of the backbone is sufficiently small so that a shift of the grafting point is only a small perturbation, especially when the chains can avoid the compressed region when necessary. We can also see the backbone as a small increase of the side chain length by a few (about 3) segments. This is a minor perturbation compared to the original system.

The topic of induced persistence length associated with the grafted chains on a backbone is less developed than the electrostatic stiffening. The finite volume of the backbone is of little importance as soon as there is some annealed character of the grafting. In principle this is good news for the co-assembled bottlebrushes which will be discussed next. Below we are interested in the formation of a bottlebrush by physisorption. In this case the chains are in equilibrium with chains in the bulk and this provides an annealing mechanism. Hence, we should expect that the phantom chain case is the relevant one to compare with.

25

C. Self-assembled bottlebrushes

Result in this section are selected to match the experimental situation we have for the DNA co-assembled bottlebrushes. Experimentally, we used C_4K_{12} protein polymers which we model here by $K_{12}A_{400}$ where A is an athermal uncharged segment and K is a segment which adsorbs onto the core, either with an adsorption energy χ_S, or by electrostatic attraction: then each segment K has a valency of $+1$. In the electrostatic binding case we consider DNA with $v = -3$, which translates to 6 negative charges per nm DNA contour length. This means that binding upto charge stoichiometry amounts to 0.5 chain per nm, or 0.25 chains per lattice unit. Below, we report adsorbed amounts computed in the two-gradient cylindrical coordinate system by

$$\theta^\sigma = \sum_z \sum_r L(r) \left(\varphi(z,r) - \varphi^b\right) \tag{27}$$

When we divide this by the chain length N we obtain the excess number of chains per unit length. Note that, by definition, the value θ^σ will go to zero in the limit of $\varphi^b \to 1$. Hence, adsorption isotherms in these units therefore typically have two regimes of behavior. As long as the bulk volume fraction is below the overlap the adsorbed amount increases with bulk volume fraction, whereas above the overlap concentration the excess adsorption has the tendency to decrease. Charge stoichiometry occurs at $\theta^\sigma \approx 100$. Experimentally, data for the binding of C_4K_{12} onto DNA are available [5]: the maximum binding goes to approximately 70% coverage at 10 mM salt and it drops to $\approx 60\%$ for 60 mM salt and to about 30% for 160 mM salt.

In Figure 5 we show the result of SCF calculations for the adsorbed amount, θ^σ, of C_4K_{12} protein polymer as a function of the volume fraction of C_4K_{12} in the bulk. The figure is in lin-log coordinates in the regime for which the bulk volume fraction remains below overlap. In this figure we see two sets of adsorption isotherms. The solid lines are for the electrostatic adsorption mechanism. The dashed curves are for the fixed adsorption energy case.

For all isotherms that lack cooperativity it is true that the slope $\partial \theta^\sigma / \partial \varphi^b$ decreases with increasing coverage. Interestingly, for the electrostatic adsorption mechanism even the slope $\partial \theta^\sigma / \partial \log \varphi^b$ decreases with coverage. This reduction in affinity is due to the adsorption mechanism. In the case of low coverage there are many free charges around the backbone and the electrostatic potential around the DNA is high and hence the driving force for

26

adsorption is strong. For a high coverage there are not many 'free' charges left around the DNA backbone. The electrostatic potential becomes low and hence the driving force for adsorption reduces. The plateau of the isotherm is found at relatively low bulk volume fractions and the plateau is below charge stoichiometry. The lower the ionic strength, the closer the isotherms approach charge stoichiometry. The isotherms are truncated just before the bulk volume fraction of the polymer reaches the overlap concentration $\varphi^b \approx 0.0025$. The maximum coverage in terms of percentage of charge stoichiometry is 0.9 for $\varphi_s = 10^{-4}$ (1 mM), 0.7 for 10 mM salt and 0.5 for 50 mM salt. These numbers are in good agreement with the experimental data mentioned above.

The set of adsorption isotherms which correspond to a fixed adsorption energy are dramatically different in shape. As each chain has only a few adsorbing segments, the adsorption energy starts at a rather high bulk volume fraction. After the Henri regime (an initial linear increase of $\theta^\sigma(\varphi^b)$) the isotherm becomes straight in lin-log coordinates, which implies logarithmic growth. The adsorbed amount grows with increasing adsorption energy at a given bulk volume fraction. It is found that θ^σ can exceed 100. At this coverage the adsorbing fragment K_{12} occupies all adsorbing sites when all the segments would be adsorbed in the so-called train conformation. However, at such high coverages the adsorbed layer also develops small loops and therefore θ^σ can exceed the monolayer coverage for the adsorbing block.

As the two sets of isotherms are dramatically different in shape, they cross each other. We have labeled in Figure 5 these crossing points for reference purposes: the numbers re-appear in Figure 6.

Figure 6 shows the persistence length of the DNA-bottlebrushes as a function of the amount of bound C_4K_{12} protein polymer, both for the electrostatic driving force as well as for the systems that have a fixed adsorption energy (dashed line), in double logarithmic coordinates. In the latter systems there is only a contribution of the adsorbed protein polymers. The persistence length data follow a power-law scaling with a slope of 1.8, which is very close to the corresponding results for chemically grafted brushes in the phantom chain limit. The value is a bit below the scaling prediction for brushes of 2. The deviation from 2 arguably is due to the fact that the chain length used, $N = 400$, for the stabilizing block is still rather short. The symbols on the curve correspond to the crossing points of the isotherms in Figure 5. Note that these points are taken from isotherms that differ
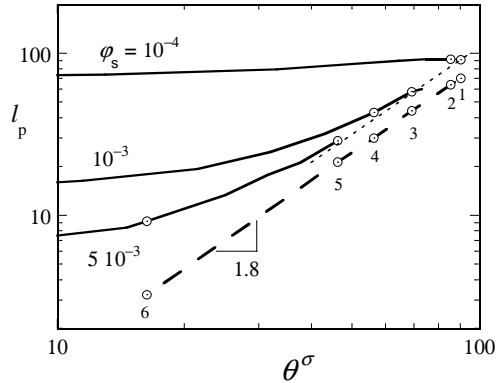
27

FIG. 6. The bending rigidity of the self-assembled bottlebrush in lattice units as a function of the amount of C_4K_{12} copolymers that are physisorbed per unit length (lattice units) onto the DNA chain in log-log coordinates. Solid lines are for the charged case. Three curves are given for ionic strengths $\varphi_s = 10^{-4}$, 10^{-3} and 5×10^{-3}, as indicated. The dashed line is for the fixed adsorption energy case. The symbols with numbers correspond to the crossings of the isotherms in Figure 5. The slope of the dashed line is 1.8. The dotted line (with same slope) is to guide the eye.

with respect to adsorption energy value. We conclude that for the persistence length only the coverage is important while both the bulk volume fraction of protein polymers and the adsorption energies (of course necessary to reach a particular coverage) are irrelevant for the stiffness.

The tunable contributions of the persistence length for the electrostatically driven bottlebrushes is more complex. In all cases the persistence length is above the value for fixed adsorption energy cases. The reason for this is clear. Apart from the brush there is a contribution due to the (residual) electric double layer. We present three curves for $l_p(\theta^\sigma)$, for different values of the ionic strength. Indeed at low polymer coverage ($\theta^\sigma << 50$) the tunable contribution to the persistence length is dominated by the electrostatic stiffening effect. The limiting values for vanishing coverages of the protein polymer of l_p decrease sharply with increasing ionic strength: its stiffening is well below 10 (lattice units) for $\varphi_s = 5 \times 10^{-3}$, about 15 for $\varphi_s = 10^{-3}$ and about 70 for $\varphi_s = 10^{-4}$. These limiting values do not exactly follow the Fixman Odijk prediction [3, 4] because the charge density on the DNA is above the Manning condensation limit. At high coverages the induced persistence length dominates the tunable contributions. This is illustrated by the dotted line which is drawn with a slope of 1.8. All three curves approach the same brush-dominated trend asymptotically

28

(dotted line).

From the above, we know that electrostatic stiffening roughly scales quadratically with linear charge density on the brush. We also know that there is a roughly quadratic scaling of the persistence length with grafting density (adsorbed amount). This means that we should expect an interpolation curve between the electrostatic stiffening limit and the brush limit without local minima or maxima. When the two limiting values are close, such as in the low ionic strength case ($\varphi_s = 10^{-4}$), there is a simple interpolation and the curve is close to horizontal. When the limiting values are further apart, we see that with decreasing adsorbed amount, the brush contribution first reduces according to the power-law scaling $l_{\mathrm{p}} \propto (\theta^\sigma)^{1.8}$ from which it starts to level off as soon as the induced persistence length becomes of the same order as the electrostatic stiffening limit.

As mentioned already the symbols on the curves correspond to the crossings of the isotherms shown in Figure 5. Labels 1 and 2 correspond to the $\varphi_s = 10^{-4}$ system, 3 and 4 for $\varphi_s = 10^{-3}$ while 5 and 6 are for $\varphi_s = 5 \times 10^{-3}$. The persistence length for all points on the electrostatically driven brush formation are higher than their corresponding point on the curve for the fixed adsorption energies. One may argue that the difference is simply the contribution of the electric double layer. However, close inspection shows that this cannot be the case. Based on the value of $l_{\mathrm{p}} \approx 8$ (lattice units) for the electrostatic stiffening at $\varphi_s = 5 \times 10^{-3}$ and $\theta^\sigma = 10$, we expect for $\theta^\sigma \approx 40$ a $16\times$ lower value (surface charge is reduced by a factor 4) of the electrostatic stiffening. Hence, for point 5, the contribution of the electrostatic stiffening must be below unity. Nevertheless, the difference in stiffening of the two points labeled 5 is still approximately 10 (lattice units)! The same applies to the difference of the persistence length for the two points labeled with 4: the observed difference for l_{p} is about 13 (lattice units), whereas the electrostatic stiffening is again expected to be less than unity. The low coverage limit at $\theta^\sigma = 10$ equals $l_{\mathrm{p}} \approx 16$, and at $\theta^\sigma \approx 56$ the electrostatic contribution should have dropped by a factor of about 25, i.e. to 0.4. The same applies for the systems with label numbered 3. The observed difference in persistence length between the charged and the uncharged systems is too large to be simply related to the electrostatic persistence length contribution, even when we account for the Manning condensation effect.

We have discussed at length that systems that can regulate the grafting position have a very low persistence length, compared to the systems for which the mobility of the grafts
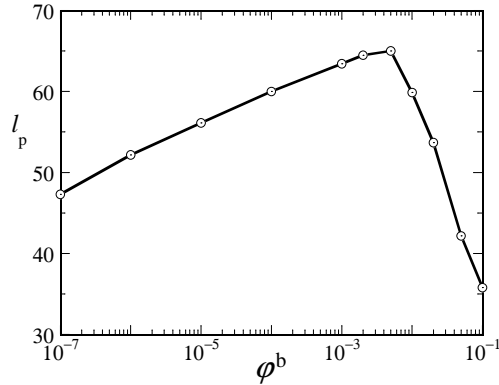
29

FIG. 7. The tunable contribution to the persistence length l_{p} in lattice units for co-assembled DNA-bottlebrushes as a function of the bulk volume fraction of C_4K_{12} for $\varphi_s = 0.001$ in lin-log coordinates. The charge $v = -3$ around the DNA chain is homogeneously distributed (cf. Figure 2F). The focus is on the behavior near the overlap concentration.

is impaired. We therefore attribute the rather high persistence length for electrostatically driven adsorption to the fact that the chains accumulate preferentially at places where the electrostatic potential is highest. When the charged DNA chain is curved, the electrostatic potential is highest in the confined convex part of the chain and lowest at the expanded concave part. Hence, there may be a small preference for the C_4K_{12} protein polymer to be attached to the confined part of the curved DNA chain. Even when this effect is small, there may be a big effect on the persistence length. Indeed the differences in l_{p} of 10 to 15 (lattice units) are significant.

The results for the tunable contributions of the persistence length of Figure 6 are for the regime where the protein-polymer concentration is in the dilute regime. In Figure 7 we show how the persistence length changes with polymer concentration for the co-assembled DNA-bottlebrush system under intermediate ionic strength conditions, i.e. $\varphi_s = 10^{-3}$ (10 mM salt). Similarly as in Figure 6 the charge density on the DNA is $v = -3$. We select the regime for which the tunable contributions of the persistence length is dominated by the bottlebrush contribution. Inspection of Figure 7 reveals that below the overlap concentration the induced persistence length increases with polymer concentration, whereas above the overlap the induced persistence length drops sharply. This result is comparable to our earlier prediction for chemically grafted bottlebrushes [42]. To explain this drop in induced persistence length, we must realize that in the bottlebrush corona the local polymer density is

30

also in the overlap regime. As soon as the free polymer concentration becomes comparable to the polymer concentration in the corona, the free polymers impose an osmotic pressure such that the stretching of the corona chains diminishes: the typical shape of the corona chains relaxes back to Gaussian conformations. When the stretching of the chains diminishes, there is no information in the corona on the exact direction of the main-chain. Hence, there is less stiffening.

V. DISCUSSION

We have discussed various models for molecular bottlebrushes and focused on the tunable contributions to the persistence length. In particular, we introduced a number of models wherein the backbone volume was accounted for. We found that the backbone volume does not play a very important role, especially in cases wherein the charge along the backbone, or the grafting density of the side chains, have a degree of freedom to adjust to the imposed curvature stress. The so-called annealed cases gave persistence lengths similar to the ideal phantom chain models. Only when rather odd models were used in which the charge or the grafting density was quenched, we saw noticeable differences. We have seen that the electrostatic driving force for co-assembly leads to surprisingly large persistence lengths for the bottlebrushes. This result was traced to the reduced tendency of electrostatically bound chains to translocate from the compressed convex to the expanded concave sides of the curved DNA chain. The increased rigidity of the bottlebrush may translate to an increase in the persistence length of perhaps 10 nm, which is significant compared to the bare persistence length of DNA of about 30 nm, and tunable values which can be of the same order of magnitude.

Our main target was to understand the behavior of our experimental system which is a bottlebrush formed by co-assembly of negatively charged double stranded DNA with a chemically well defined protein polymer, C_4K_{12}, which has 12 positively charged lysines connected to 400 aa long coil-like chain. Our co-assembled bottlebrush was found to show lyotropic behavior, which is in fact a rare case for bottlebrush systems.[5] One might argue that naked DNA by itself forms liquid crystalline phases at sufficiently high concentration, and that it therefore is not too surprising that the corresponding bottlebrushes do the same. However, we have many failed attempts that use DNA as a backbone to make supramolecular bottle-

31

brushes, but have different side chains than the C_4K_{12} protein polymer. Our numerical SCF analysis now gives us more insights why it is not so easy to find co-assembled bottlebrushes with lyotropic properties.

For liquid crystalline behavior the l_p/D ratio must be significantly larger than unity. We have shown elsewhere that our bottlebrushes have a diameter in the order of 20 to 30 nm, which is about 10 times larger than the naked DNA. Clearly the co-assembled bottlebrushes did not increase the persistence length by the same factor of 10 compared to the naked DNA (including electrostatic stiffening). The above shows that at low ionic strength the induced persistence length of the brush simply replaces the electrostatic stiffening. At higher ionic strength the induced persistence length is larger than the electrostatic stiffening and thus l_p can be increased. Including the bare persistence length, we might have increased the overall persistence length from about 50 nm to perhaps 80 nm, but that's all. Apparently the l_p/D remained just large enough that lyotropic behavior was kept.

We have seen in our experiments that overdosing the system with C_4K_{12} such that the free polymer concentration is above overlap, reduces the tendency to form lyotropic phases.[5] The results shown in Figure 7 explain this observation: to have lyotropic co-assembled bottlebrushes one should avoid having a high polymer concentration in the bulk.

We may now speculate why, in nature, bottlebrushes are used in lubrication applications. For lubrication applications it appears necessary to prevent pressure induced crystallisation. In other words, with increased compression forces, e.g. by freely dispersed polymers in solution, the system should remain liquid and isotropic. Bottlebrushes become more flexible when compressed and therefore are more likely to mix into an isotropic polymer melt rather than choose for a separated oriented liquid crystalline phase when embedded in a semi-dilute or concentrated polymer solution.

The best conditions to form lyotropic co-assembled DNA-bottlebrushes as predicted by the numerical SCF modeling are: (i) polymer concentrations around the overlap concentration (ii) low ionic strength condition (when the ionic strength is very low the stiffening can be both due to the electrostatic double layer or to the brush), (iii) Long side chains with short anchor groups, (iv) polymers with a positive virial coefficient which endows stretching of the side chains.

We have seen that freely dispersed polymers above the overlap concentration have a negative effect on the bottlebrush stiffness. We expect the reduced stiffening of the bottle-

32

brushes to also occur upon compressing bottlebrushes, e.g., by increasing the bottlebrush concentration. Hence solutions of bottlebrushes above the overlap concentration may have compressed coronas and hence a reduced rigidity. We expect that this is a general effect and does not only apply to co-assembled bottlebrushes. For example, classical chemically grafted bottlebrushes will experience similar compression induced flexibilisation, and may fail to produce anisotropic phases upon increasing the concentration. This might very well be the reason why it is so difficult for bottlebrush systems to become liquid crystalline. A similar conclusion may already be found in the early bottlebrush literature [43] and there is also some recent experimental evidence for this phenomenon [44, 45] Bottlebrush systems in nature often do not become liquid crystalline and this might very well be because their architecture is actually preventing this.[46]

VI. CONCLUSION

We have used a numerical self-consistent field theory to analyze the electrostatic stiffening as well as the bottlebrush induced stiffening in molecularly realistic models for macromolecular bottlebrush systems in the dilute regime. We found that the finite volume of the backbone is unimportant as long as the charge density or the brush grafting density is annealed, i.e. can adjust itself to relax the bending stresses. Our focus was to model co-assembled DNA-bottlebrushes which are formed by binding a well-defined protein polymer (C_4K_{12}) to dsDNA by electrostatic driving forces. We distinguish three terms to the overall persistence length: (i) the bare or intrinsic value, (ii) an induced persistence length caused by the bottlebrush side chains, (iii) and an electrostatic contribution from the electric double layer around the DNA. In general, we found that when the side chains are bound to the DNA, the electrostatic stiffening is approximately replaced by the induced persistence length contribution. In other words, both terms are of the same order of magnitude. Interestingly, for electrostatically driven co-assembled DNA-bottlebrushes a remarkably high persistence length is found because the side chains have a low tendency to redistribute upon bending. This is because the chains bind best to the places where the electrostatic potential is highest, i.e. on the compressed convex side, rather than on the expanded concave side. This might be one of the reasons why our co-assembled DNA-bottlebrush system shows liquid crystalline behavior. The calculations have furthermore shown that freely dispersed poly-

mers above the overlap concentration can reduce the persistence length of bottlebrushes. We speculated that the crowding of bottlebrushes will induce a reduction of the stiffness as well, because both presence of free polymers and confinement cause a reduction of the stretching in the side chains. The loss of stretching leads to a flexibilisation of the chain as a whole. This flexibilisation mechanism may yet be another reason why there are so few reports on bottlebrushes in the literature that feature lyotropic behavior.

VII. ACKNOWLEDGEMENT

---

[1] A. N. Semenov and A. R. Khokhlov, Usp. Fiz. Nauk (Soviet Physics - Uspekhi) **156**, 427 (1988).

[2] S. Brinkers, H. R. C. Dietrich, F. H. de Groote, I. T. Young, and B. Rieger, J. Chem. Phys. **130**, 215105 (2009), http://dx.doi.org/10.1063/1.3142699.

[3] J. Skolnick and M. Fixman, Macromolecules **10**, 944 (1977), http://dx.doi.org/10.1021/ma60059a011.

[4] T. Odijk, J. Polym. Sci. Part B Polym. Phys. **15**, 477 (1977).

[5] I. M. Storm, M. Kornreich, A. Hernandez-Garcia, I. K. Voets, R. Beck, M. A. Cohen Stuart, F. A. M. Leermakers, and R. de Vries, J. Phys. Chem. B. **119**, 4084 (2015).

[6] I. K. Voets, R. de Vries, R. Fokkink, J. Sprakel, R. P. May, A. de Keizer, and M. A. Cohen Stuart, Eur. Phys. J. E **30**, 351 (2009).

[7] A. Hernandez-Garcia, M. W. T. Werten, M. M. A. Cohen Stuart, F. A. de Wolf, and R. de Vries, Small **8**, 3491 (2012).

[8] G. H. Fredrickson, Macromolecules **26**, 2825 (1993).

[9] F. Livolant and A. Leforestier, Prog. Polym. Sci. **21**, 1115 (1996).

[10] M. Wintermantel, K. Fischer, M. Gerle, R. Ries, M. Schmidt, K. Kajiwara, H. Urakawa, and I. Wataoka, Angew. Chem. Int. Ed. **34**, 1472 (1995).

[11] Y. Tsukahara, Y. Ohta, and K. Senoo, Polymer **36**, 3413 (1995).

[12] Y. Nakamura, M. Koori, Y. Li, and T. Norisuye, Polymer **49**, 4877 (2008).

[13] X. Li, H. ShamsiJazeyi, S. L. Pesek, A. Agrawal, B. Hammouda, and R. Verduzco, Soft Matter **10**, 2008 (2014).

[14] P. A. Janmey, J.-F. Leterrier, and H. Herrmann, Curr. Opin. Colloid Interface Sci. **8**, 40 (2003).

[15] J. B. Jones and C. R. Safinya, Biophys. J. **95**, 823 (2008).

[16] R. Beck, J. Deek, and C. R. Safinya, Biochem. Soc. Trans. **40**, 1027 (2012).

[17] R. Beck, J. Deek, J. B. Jones, and C. R. Safinya, Nat. Mater. **9**, 40 (2009).

[18] G. S. Manning, J. Chem. Phys. **51**, 924 (1969).

[19] L. Feuz, F. A. M. Leermakers, M. Textor, and O. V. Borisov, Macromolecules **38**, 8891 (2005).

[20] T. M. Birshtein, P. A. Iakovlev, V. M. Amoskov, F. A. M. Leermakers, E. B. Zhulina, and O. V. Borisov, Macromolecules **41**, 478 (2008), http://dx.doi.org/10.1021/ma071303h.

[21] I. V. Mikhailov, A. A. Darinskii, E. B. Zhulina, O. V. Borisov, and F. A. M. Leermakers, Soft Matter **11**, 9367 (2015).

[22] V. A. Andreev and A. I. Victorov, J. Chem. Phys. **132**, 054902 (2010), http://dx.doi.org/10.1063/1.3298991.

[23] Y. Lauw, F. Leermakers, and M. Cohen Stuart, J. Phys. Chem. B **111**, 8158 (2007), http://dx.doi.org/10.1021/jp071756o.

[24] G. J. Fleer, M. A. Cohen Stuart, J. M. H. M. Scheutjens, T. Cosgrove, and B. Vincent, *Polymers at interfaces* (Chapman and Hall, London, 1993).

[25] A. Y. Grosberg and A. R. Khokhlov, AIP press. Woodbury, NY (1994).

[26] W. Helfrich, Zeitschrift fur Naturforschung. Teil C: Biochemie, Biophysik, Biologie, Virologie **28**, 693 (1973).

[27] M. Saariaho, O. Ikkala, I. Szleifer, I. Erukhimovichm, and G. ten Brinke, J. Chem. Phys. **107**, 3267 (1997).

[28] M. Saariaho, I. Szleifer, O. Ikkala, and G. ten Brinke, Macromol. Theory Simul. **7**, 211 (1998).

[29] H.-P. Hsu, W. Paul, and K. Binder, Macromol. Theory Simul. **20**, 510 (2011).

[30] D. G. Angelescu and P. Linse, Macromolecules **47**, 415 (2014), http://dx.doi.org/10.1021/ma4021246.

[31] M. Fixman, J. Phys. Chem. B **114**, 3185 (2010), http://dx.doi.org/10.1021/jp1005742.

[32] J.-L. Barrat and F. Joanny, "Theory of polyelectrolyte solutions," in *Advances in Chemical Physics* (John Wiley & Sons, Inc., 2007) pp. 1–66.

[33] N. J. Bjerrum, **7**, 1 (1926).

[34] T. L. Hill, *An introduction to statistical thermodynamics* (Addison-Wesley, London, 1960).

[35] J. Lyklema, *Fundamentals of Interface and colloid science*, Vol. 1 (Academic Press, 1991).

[36] P. Flory, *Principles of polymer chemistry* (Cornell University Press, 1953).

[37] R. D. Groot, J. Chem. Phys. **118**, 11265 (2003).

[38] O. A. Evers, J. M. H. M. Scheutjens, and G. J. Fleer, Macromolecules **23**, 5221 (1990).

[39] I. M. Lifshitz, A. Y. Grosberg, and A. R. Khokhlov, Rev. Mod. Phys. **50**, 683 (1978).

[40] S. F. Edwards, Proc. Phys. Soc. **85**, 613 (1965).

[41] F. A. M. Leermakers, J. Chem. Phys. **138**, 154109 (2013).

[42] I. M. Storm, M. Kornreich, I. K. Voets, R. Beck, R. de Vries, M. A. Cohen Stuart, and F. A. M. Leermakers, Soft Matter **12**, 8004 (2016).

[43] O. Borisov, T. Birshtein, and Y. Zhulina, Polymer Science U.S.S.R. **29**, 1552 (1987).

[44] S. Bolisetty, S. Rosenfeldt, C. N. Rochette, L. Harnau, P. Lindner, Y. Xu, A. H. E. Müller, and M. Ballauff, Colloid and Polymer Science **287**, 129 (2008).

[45] S. Rathgeber, T. Pakula, A. Wilk, K. Matyjaszewski, H. il Lee, and K. L. Beers, Polymer **47**, 7318 (2006).

[46] J. Klein, Polym. Adv. Technol. **23**, 729 (2012).